TiO_2 functionalized nanofibrous membranes for removal of organic (micro)pollutants

*Jozefien Geltmeyer[a], Helena Teixido[a], Mieke Meire[b], Thibaut Van Acker[d], Koen Deventer[c], Frank Vanhaecke[d], Stijn Van Hulle[e], Klaartje De Buysser[b], Karen De Clerck[a,]**

[a] Fibre and Colouration Technology Research Group, Department of Textiles, Faculty of Engineering and Architecture, Ghent University, Technologiepark 907, 9052 Ghent, Belgium, Karen.DeClerck@UGent.be, Phone: +32 (0)92645740, Fax: +32(0)92645846

[b] Sol-gel Centre for Research on Inorganic Powders and Thin Films Synthesis, Department of Inorganic and Physical Chemistry, Faculty of Sciences, Ghent University, Krijgslaan 281 S3, 9000 Ghent, Belgium

[c] Doping Control Laboratory, Ghent University, Technologiepark 30, 9052 Ghent, Belgium

[d] Department of Analytical Chemistry, Faculty of Sciences, Ghent University, Krijgslaan 281 S12, 9000 Ghent, Belgium

[e] LIWET, Department of Industrial Biological Sciences, Ghent University Campus Kortrijk, Graaf Karel de Goedelaan 5, B-8500 Kortrijk, Belgium

Abbreviations[1]

[1] PA 6: polyamide 6, MB: Methylene Blue, IL: inline, DC: dip-coating, H: hydrophilic

ABSTRACT Titania has already proven its added value for air and water treatment. The higher the surface-to-volume area, the better the performance of the TiO_2 photocatalyst. These nanoparticles are typically applied in a slurry form. The use of titania nanoparticles in suspension has, however, multiple disadvantages such as a high turbidity and complex recovery of the photocatalyst after use. Therefore, immobilization of titania nanoparticles on a porous support such as a nanofibrous membrane, can be highly valuable for water treatment. These TiO_2 functionalized nanofibrous membranes may be used not only in a membrane separation reactor, but also in a contact reactor. In this study, TiO_2 nanoparticles were immobilized on both polymer (polyamide 6) and ceramic (silica) nanofibrous membranes. Polymer nanofibers are chosen as they are the state-of-the-art material, silica nanofibers on the contrary are less studied but show additional advantages due their excellent chemical and thermal stability and can thus offer a clear benefit for a wider range of applications. Two immobilization techniques were used, namely inline functionalization and dip-coating. Inline functionalization showed to be the preferred method for polyamide 6 nanofibrous membranes, dip-coating for silica nanofibrous membranes. Complete degradation of isoproturon, an actual concern in water treatment, is shown. Even the widely available commercial TiO_2 nanoparticles allowed for a complete isoproturon removal as the result of a correct immobilization process on nanofibrous materials. This clearly opens up the high value of TiO_2 functionalized nanofibrous membranes for organic (micro)pollutants removal.

KEYWORDS TiO_2 nanoparticles, photodegradation, polyamide nanofibers, silica nanofibers, isoproturon

1. INTRODUCTION

Titania, a well-known photocatalyst, is widely used because of its great availability, low cost, non-toxicity, chemical and thermal stability [1]. One of the most interesting properties of titania

is its photocatalytic activity under UV irradiation, producing highly oxidative hydroxyl radicals capable of oxidizing many organic (micro)pollutants [2]. This results in many applications such as self-cleaning surfaces, antibacterial surfaces, air purification and water purification [3–6]. Since many of the applications rely on surface related phenomena, a high specific surface area is desired as it enhances the performance of the photocatalyst. TiO_2 nanoparticles are thus known to show greater photocatalytic properties compared to their bulk counterpart [7,8].

Phenylurea herbicides are generally applied for agricultural applications. Isoproturon is one of the most used herbicides in Europe and due to its water solubility, low chemical and biological degradation it contaminates surface and ground water [9,10]. Heterogenous photocatalysis using TiO_2, has been considered as highly promising for waste water treatment and degradation of these herbicides [11,12]. Additionally, removal of organic components present in industrial, highly acidic effluents remains a major issue as well, which can also be tackled using TiO_2. Photocatalytic reactor configurations for water treatment can be classified into two types depending on the state of the photocatalyst: reactors with suspended photocatalyst particles (slurry reactors) (1) and reactors with immobilized photocatalyst particles (2). A major disadvantages of slurry type reactors (type 1) is the additional post-separation step of the photocatalyst. An increased interest is thus seen in immobilizing the TiO_2 nanoparticles on a porous, inert support [13–17].

Nanofibrous membranes, obtained via the electrospinning process, have a high specific surface area, high porosity and small pore sizes. These unique properties make these non-woven membranes ideal for a wide range of filtration applications [18]. Moreover, they show to be an ideal highly porous support for immobilization of TiO_2 nanoparticles. Via the electrospinning process both polymeric as ceramic nanofibrous membranes can be produced [19–21]. Polymer nanofibrous membranes functionalized with TiO_2 nanoparticles have already shown to be promising for photodegradation of dissolved organic matter, humic acids and

bacteria [3,22,23]. Ceramic membranes, although less exploited so far, have many advantages over polymeric membranes for filtration applications, since they have typically superior thermal properties, and a better resistance against corrosion and chemicals [24]. These membranes can thus be used for highly acidic effluents. Silica nanofibers have recently shown their added value for removal of heavy metal ions and dyes via sorption [25–27]. So far they have not yet been exploited to study the removal of micro pollutants. Functionalization of these nanofibrous membranes with TiO_2 nanoparticles results in an added functionality for removal/degradation of organic components. Additionally, functionalization with TiO_2 prevents fouling of the membranes, which is a major concern in membrane use for water treatment [24,28]. Thus TiO_2 functionalized ceramic nanofibers will be exploited here for the removal of micro pollutants.

The simplest approach for functionalization with TiO_2 nanoparticles is the addition of a chosen amount of the particles to the solution prior to electrospinning, namely inline functionalization. An alternative method is post-functionalization, where the membranes are functionalized with TiO_2 after production. In this study, the dip-coating process will be studied as a post-functionalization method. Both functionalization methods have their advantages and disadvantages. Inline functionalization is an easy and straightforward, one-step functionalization method, resulting in TiO_2 nanoparticles which are distributed inside the nanofibers. Dip-coating, on the contrary, is a two-step process resulting in the presence of the nanoparticles on the surface of the nanofibers and making them more accessible to the pollutants. Three challenges are encountered during surface modification, being uniformity, coating without affecting the pore sizes and possibility for industrial upscaling [18].

In this work, commercial Degussa P25 TiO_2 nanoparticles are immobilized in and on a highly porous nanofibrous support. Commercial Degussa P25 TiO_2 nanoparticles have already proven their value as photocatalyst for water treatment, but proper immobilization remains vital as it

increases the applicability of these nanoparticles. Therefore, in this study both polymeric (polyamide 6) and ceramic (silica) nanofibrous membranes are functionalized with these TiO_2 nanoparticles. First, the TiO_2 loading of inline and dip-coated nanofibrous membranes are quantified using TGA, XRD and ICP-OES. Next, the photocatalytic behavior is tested by decoloring of methylene blue, an ideal test compound for a first screening of the produced membranes and their degradation efficiency. Finally, the true degradation potential of micro pollutants is tested on isoproturon using a basic set-up. Both UV-Vis spectroscopy and LC-MS are used for evaluation of the degradation of the pollutants. The removal of isoproturon is a real concern in water treatment today in view of discharge to the environment and has not yet been solved adequately. It is believed that commercial TiO_2 nanoparticles may be highly valuable when immobilized on porous polyamide or silica nanofibrous membranes for removal of various organic (micro)pollutants. Moreover, these membranes are applicable in various water treatment set-ups such as contact reactors or membrane separation reactors.

2. EXPERIMENTAL SECTION

2.1 Materials. Titanium (IV) oxide (Degussa P25) was obtained from Sigma-Aldrich. It is a standard material in the field of photocatalytic reactions, having a primary particle size of 21 nm and a specific surface area of 35-65 m^2/g. The sol-gel precursor tetraethoxysilane (TEOS, reagent grade 98%) and hydrogen chloride (HCl, 37%) used as catalyst for the sols, were both obtained from Sigma-Aldrich and used as received. The solvent absolute ethanol was obtained from Fiers. Polyamide 6 (PA 6) pellets were provided by Sigma-Aldrich and used as received. The solvents formic acid (98 v%) and acetic acid (99.8 v%) were supplied by Sigma-Aldrich. The dye methylene blue and the herbicide isoproturon were also provided by Sigma-Aldrich.

2.2 Electrospinning of nanofibers. Polyamide solutions for electrospinning were prepared by dissolving 13 wt% and 16 wt% of PA 6 in a 50:50 v% formic acid:acetic acid solvent

mixture. The sols were prepared using the methodology described in previous work [29–31]. The sols were prepared from a mixture of TEOS:ethanol:H_2O:HCl with a molar ratio of respectively 1:2:2:0.01. Firstly, TEOS and ethanol were mixed. Secondly, aqueous HCl was added to the solution under vigorous stirring. After completion of the hydrolysis reactions (exothermic process) the sols were heated under stirring at 80°C. An Allihn set-up was used allowing the ethanol to reflux during 16 h. Finally, a rotary evaporator was used to evaporate the ethanol until a desired sol viscosity, in between 100 and 200 mPa.s, was reached.

Prior to electrospinning the viscosity of the solutions was measured using a Brookfield viscometer LVDV-II. The electrospinning experiments were executed on a mononozzle set-up with a rotating drum collector. For the electrospinning of the 16 wt% polyamide solutions a tip-to-collector distance (TCD) of 6 cm was used, a flow rate of 2 mL h^{-1} and a voltage in between 21 and 25 kV. The electrospinning of the 13wt% PA 6 solution was carried out with a TCD of 10 cm, flow rate of 0.5 ml h^{-1} and a voltage in between 20 and 25 kV to obtain a stable process. For the electrospinning of the silicon oxide sols the TCD was fixed at 15 cm, the flow rate at 1 mL h^{-1} and the voltage was adjusted in between 20 and 24 kV to obtain a stable electrospinning process. All the experiments were executed at a relative humidity of 34% RH ± 10% of and a room temperature of 22°C ± 2°C. Nanofibrous membranes with a density of ± 10 g/m^2 were obtained.

2.3 Functionalization of nanofibers. Inline (IL) functionalization was carried out by adding varying amounts of TiO_2 nanoparticles to the electrospinning solutions prior to electrospinning. For the lower TiO_2 loadings (0.2 wt% - 5 wt%), TiO_2 powder was added after preparation of the electrospinning solutions, the solutions were first stirred with a magnetic stirrer during 0.5 h and next ultrasonicated for 0.5 h, resulting in a homogenous dispersion of the nanoparticles. These low TiO_2 loadings had no influence on the electrospinning process. Electrospinning of the higher TiO_2 load (35 wt%) was only possible when the amount of PA 6 in the formic

acid/acetic acid solutions was lowered from 16 wt% to 13 wt% PA 6. To prepare the 35 wt% TiO_2 inline functionalized PA 6 solution, the TiO_2 nanoparticles were first homogenously mixed in the solvent mixture by ultrasonication, next the polymer pellets were added and the solution was stirred for 6h. The electrospinning parameters were optimized as described above.

The amount of TiO_2 added is expressed as a weight percentage relative to the total weight of polyamide 6 and TiO_2, or silica and TiO_2. To indicate the relative amounts of TiO_2 added to the silica nanofibers it was assumed that complete crosslinking of the TEOS took place resulting in a SiO_2 network.

Aqueous TiO_2 nanoparticle suspensions (0.12 mol L^{-1}, 0.34 mol L^{-1} and 0.5 mol L^{-1}) were dip-coated on the nanofibrous membranes at room temperature and at a coating speed of 102.8 mm/min, using a computer controlled dip-coating unit (KSV Instruments). Dip-coating was carried out in a clean room facility (class 100 000/1000). Samples dip-coated (DC) with a 0.12 mol L^{-1} and 0.5 mol L^{-1} TiO_2 aqueous suspension were immersed for 3 min. Samples dip-coated with a 0.34 mol L^{-1} TiO_2 aqueous suspension were immersed for 10 min. Both hydrophobic as well as hydrophilic silica nanofibrous membranes were dip-coated. Hydrophilic membranes functionalized via dip-coating are denoted with a H. The as-coated membranes were first dried at room temperature for 24 h, after which the samples were cured during 30 min at 100°C.

2.4 Characterization of nanofibrous membranes. The morphology and the diameters of the nanofibers were examined using a FEI Quanta 200 F Scanning Electron Microscope (SEM) at an accelerating voltage of 20 kV. Prior to analysis the samples were coated using a sputter coater (Emitech SC7620, Au coating). Image J software was used to determine the nanofiber diameters by taking an average of 50 measurements per sample. Thermogravimetric analysis of the TiO_2 functionalized PA 6 membranes were performed on a Netzsch STA449 FR Jupiter set-up. The samples were heated at a rate of 10°C min^{-1} from room temperature to 800°C under air.

Details on Inductively Coupled Plasma Optical Emission Spectroscopy (ICP-OES) analysis, X-ray Diffraction (XRD) analysis and Tauc plot construction are given in the Supporting information.

2.5 Photocatalytic activity test. The photocatalytic activity of the membranes was evaluated by photodegradation of aqueous solutions of both methylene blue (4.2 mg L^{-1}) and isoproturon (5 and 10 mg L^{-1}) under UV irradiation. Methylene blue (MB) was simply dissolved in distilled water, isoproturon was first dissolved in aceton at a concentration of 1000 mg L^{-1}. This solution was then diluted with distilled water to a concentration of 5 or 10 mg L^{-1}. A schematic diagram of the used set-up is given in Figure 1. For each type of membrane, three samples were tested simultaneously. The samples were fixed in a sample holder and immersed in a tempering beaker (15 °C) containing the MB or isoproturon solution. The samples were illuminated from a distance of 13 cm by a 300 W Osram Ultra-Vitalux lamp, emitting radiation (mainly UV-A, similar to sunlight) with an intensity of about 5 mW/cm^2. The light emission profile of the Osram Ultra-Vitalux lamp is shown in Figure S1. To stabilize the power of its emission spectrum the lamp was switched on 1 h before starting the photocatalytic test. To ensure the attainment of the ad/absorption equilibrium the samples were immersed in the solutions 24 h prior to the photocatalytic test. The methylene blue decoloring and isoproturon degradation were followed by measuring the transmission spectra of the solutions after 0 h, 1 h, 2 h, 4 h, 6 h using a Perkin-Elmer Lambda 900 UV-Vis spectrophotometer or via Liquid Chromatography – Mass Spectrometry (LC-MS). The photocatalytic degradation rate of various organic compounds over TiO_2 usually follows pseudo first-order reaction kinetics, which is described by equation (1). C is the concentration of MB or isoproturon after a specific UV irradiation time t, C_0 is the initial concentration and k is the rate constant of the reaction.

$$\ln\left(\frac{C}{C_0}\right) = -kt \qquad (1)$$

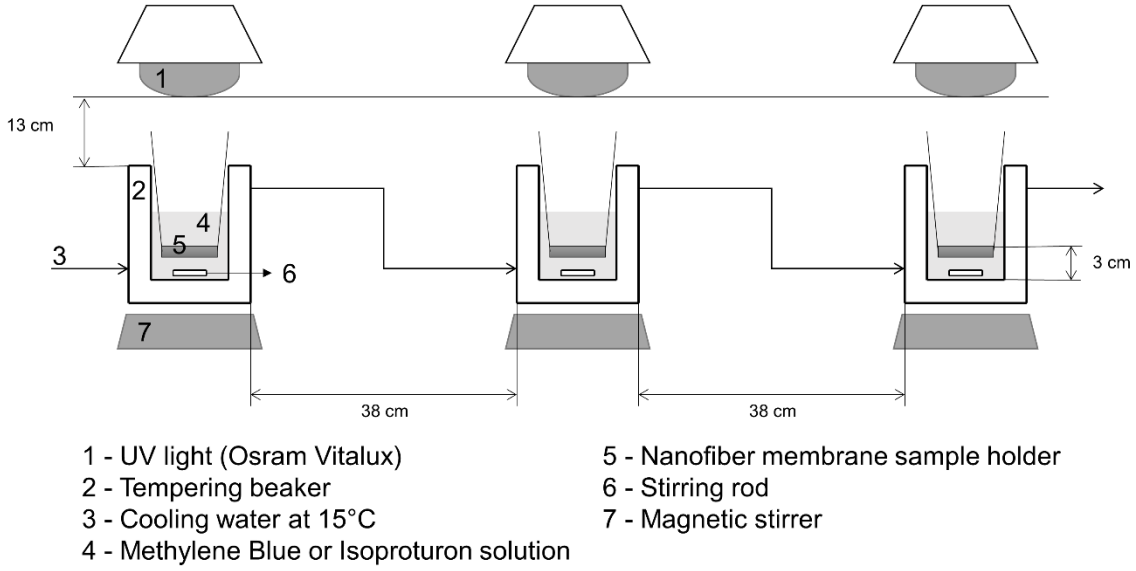

Figure 1 Schematic diagram of photocatalytic set-up

The LC-MS system consisted of a Surveyor HPLC coupled to a Quantum Discovery mass spectrometer (both from Thermo-Scientific, San Jose, CA, USA) equipped with an electrospray-source (ESI), operated in full scan positive ionization mode. Prior to analysis, samples were diluted twice with methanol (MeOH). Subsequently 1 µL was injected. Separation was performed on an Omnispher C18 column 50 x 3 mm (3 µm particle size) protected with a guard column 10 x 2 mm (both from Varian, Sint-Katelijne-Waver, Belgium). The mobile phase consisted of water and MeOH, both containing 0.1% acetic acid and 1mM ammonium acetate. A gradient program was used to elute the isoproturon. After analysis the protonated molecular ion of isoproturon (m/z 207) was extracted from the chromatograms and peak heights were plotted in function of time.

3. RESULTS AND DISCUSSION

3.1 Characterization of TiO_2 functionalized membranes

An in-depth characterization of the nanofibrous membranes and their TiO_2 loading is indispensable for a correct interpretation of the photocatalytic behavior of the produced membranes. The influence of the TiO_2 addition on the resulting nanofiber morphology was

evaluated via SEM, Figure 2. Uniform membranes were obtained (Figure 2 a,b) and fiber diameters of 222 ± 49 nm were measured for inline (IL) functionalized 2.5 wt% TiO_2 PA 6 membrane, being in line with PA 6 nanofibers without TiO_2 loading, 198 ± 47 nm, and previous research [3,32]. Smaller diameters, 98 ± 17 nm, were measured for the 35 wt% PA 6 sample, since a lower concentration of polymer was present in the solution [33,34]. The presence of TiO_2 is not visible for the low amounts (Figure 2 a), opposed to the 35 wt% PA 6 sample for which the TiO_2 particles are clearly visible, with the formation of clusters or beads (Figure 2 b).

Inline functionalization of the silicon oxide sols was possible up to 2 wt%. SEM images are shown of 0.2 wt% and 2 wt% TiO_2 loaded silica nanofibers. These samples have diameters of 346 ± 44 nm and 321 ± 165 nm, which are again largely unaltered compared to non-functionalized silica nanofibers (302 ± 83 nm) prepared in this work and in previous research [29,30]. At a TiO_2 loading of 2 wt% beads started to become present in the resulting nanofibers. It was not possible to further increase the TiO_2 loading of these membranes by inline functionalization when the same sol preparation procedure was used.

Post-functionalization via dip-coating (DC) was examined since it allows deposition of TiO_2 nanoparticles only at the surface of the nanofibers. This makes the TiO_2 nanoparticles more accessible to the pollutants in the water. However, blocking of the pores of the membranes may be a drawback together with the easier wash-out of TiO_2. Again the membranes were screened using SEM and the comparison was made between PA 6 and silica nanofibrous membranes. For the polyamide 6 membranes an increased loading is seen with increasing concentration of the solution used for dip-coating (Figure 2 c,d), which was also confirmed with TGA (Table 1). Moreover, the pores of the PA 6 membranes seem to become blocked upon functionalization with a 0.5 M TiO_2 solution. Due to their low affinity for polyamide the TiO_2

nanoparticles tend to form clusters and upon increasing concentration these clusters block the pores of the membranes.

Dip-coating of the silica nanofibers also resulted in an increased loading with an increasing concentration of the dip-coating solution. The silica nanofibers can change their hydrophilicity in time [31]. Therefore, both hydrophobic and hydrophilic samples were dip-coated, which resulted in a significant difference in TiO_2 loading (Figure 2 f,g and Table 1). Due to their high affinity for silica, the TiO_2 nanoparticles are much better distributed along the nanofibers compared to polyamide 6, resulting in only a minimal pore blocking of these silica nanomembranes. This is an important advantage if membrane separation reactors are aimed for as a pore blocking is too be minimized for an optimal reactor performance.

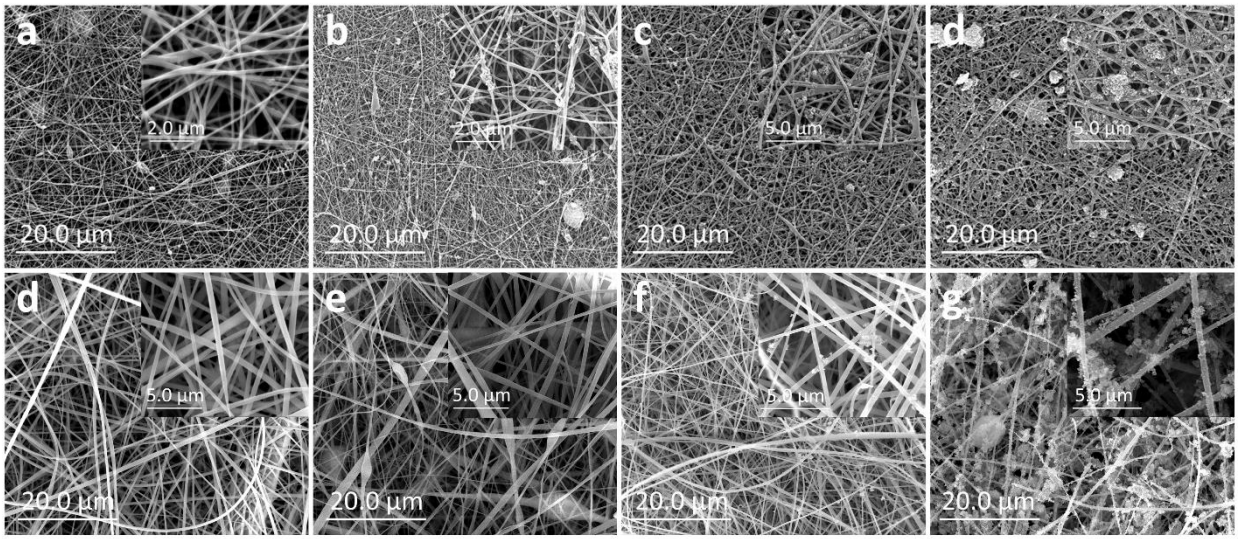

Figure 2 SEM images of polyamide 6 inline functionalized with (a) 2.5 wt% and (b) 35 wt%, post-functionalized polyamide 6 membranes with (c) 0.12 mol L^{-1} and (d) 0.5 mol L^{-1} TiO_2 solution, silica inline functionalized with (d) 0.2 wt% and (e) 2 wt%, and silica post-functionalized with 0.34 mol L^{-1} TiO_2 solution as (f) hydrophobic membrane and (g) hydrophilic membrane.

Table 1 Quantification of TiO_2 loading for PA 6 and silica nanofibrous membranes functionalized inline or via dip-coating via ICP-OES and TGA (TiO_2 quantification is not

possible via calculation for dip-coated membranes, TGA is not a valid tool for TiO_2 quantification of silica membranes) (IL: inline, DC: dip-coating and H: hydrophilic, the amount of TiO_2 added is expressed as wt% for IL samples, for the DC samples the concentration of TiO_2 in the coating solution is denoted in M (mol L^{-1})).

		Calculated amount (mg Ti g^{-1} sample)	**ICP-OES (mg Ti g^{-1} sample)**	**TGA (mg Ti g^{-1} sample)**
PA 6	IL 0.5 wt%	3	3.72	-
	IL 2.5 wt%	15	-	31.2
	IL 5 wt%	29	41.2	45
	IL 35 wt%	200	-	187
	DC 0.12 M	-	39.1	42
	DC 0.5 M	-	-	61.7
Silica	IL 0.2 wt%	1.12	0.843	-
	IL 2 wt%	11	8.81	-
	DC 0.12 M	-	8.89	-
	DC 0.34 M	-	23.5	-
	H DC 0.34 M	-	143.1	-

Quantification of the amounts of Ti/TiO_2 present in or on the nanofibers was carried out using multiple techniques. TGA was used for PA 6 membranes, XRD was used for silica membranes and ICP-OES was used for both. An overview of the results obtained via ICP-OES and TGA are shown in Table 1. The amounts of TiO_2 present in the inline functionalized membranes was, as expected, in line with the calculated amounts. With increasing concentration of TiO_2 in the dip-coating solutions, an increase in TiO_2 loading on the membranes was measured, which was also confirmed via SEM (Figure 2 c,d). Via XRD an amount of 2.19 wt% $TiSiO_4$ was determined for the 2 wt% inline functionalized silica membrane, being in line with the calculated amounts and ICP-OES results. A substantial higher

TiO_2 loading through dip-coating was noted for the hydrophilic silica samples over the hydrophobic samples.

In summary, successful functionalization of both PA 6 and silica nanofibrous membranes was carried out using both inline functionalization and dip-coating and their TiO_2 load was quantified. The photocatalytic behavior of these membranes is evaluated next to identify the most promising membranes for isoproturon degradation.

3.2 Photocatalytic behavior of TiO_2 functionalized membranes

The photocatalytic behavior of the TiO_2 functionalized nanofibrous membranes was evaluated subsequently via Tauc plots and the decoloring of methylene blue. The properties of the TiO_2 semi-conductor present in the samples was verified by plotting their Tauc plot (Figure 3), following the method reported by López *et al* [35]. The estimated band gap energies (E_g) were all in the range 3.18 - 3.30 eV, which is close to the value of 3.2 eV being extensively reported for the commercial P25 TiO_2 nanoparticles [35]. UV-A light, emitted by the chosen Osram Ultra-Vitalux lamp, is thus sufficient to overcome this band gap energy. It can be concluded that the properties of the semi-conductor do not change by incorporation in both the PA 6 and silica nanofibrous membranes.

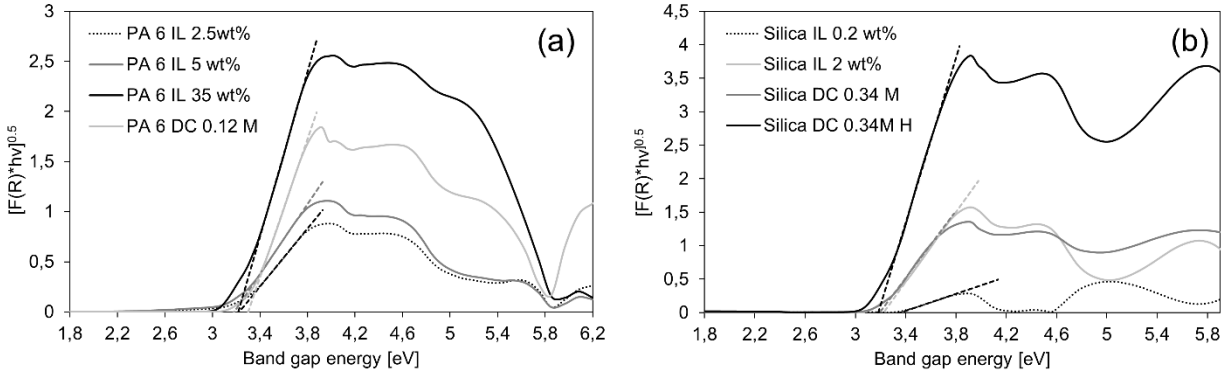

Figure 3 Tauc plot illustrating the band gap of the TiO_2 semiconductor present in the different samples: PA 6 membranes (a) and silica membranes (b) being close to 3.2 eV. (IL: inline, DC:dip-coating and H: hydrophilic); the amount of TiO_2 added is expressed as wt% for IL

samples, for the DC samples the concentration of TiO_2 in the coating solution is denoted in M (mol L^{-1}).

The photocatalytic activity of the functionalized PA 6 and silica nanofibrous membranes was further characterized by their decoloring of a methylene blue (MB) solution. The decoloring of MB is typically used as a probe to demonstrate the activity of a photocatalyst. Since it is generally accepted that the decoloring of MB follows a pseudo first-order kinetic mechanism, the photocatalytic activity of the samples was calculated from the logarithmic plots of the pseudo first-order degradation rate of the MB solutions in contact with the functionalized membranes (Figure 4). The photolysis of MB under UV light without sample present and the decoloring of the MB solution by non-functionalized samples is also plotted, to demonstrate clearly the influence of the added TiO_2 nanoparticles. The rate constants and t_{90} values given in Table 2 indicate the differences in photocatalytic activity of all samples.

Use of non-functionalized membranes resulted in a low removal of MB attributable to a combined effect of MB photolysis and MB ab-/adsorption. The inline addition of TiO_2 to the PA 6 samples resulted in a significant increased removal due to degradation by the photocatalyst. Yet, the inline addition of TiO_2 to the silica membranes did not significantly change the removal rate compared to non-functionalized samples. This can be explained by the shielding of TiO_2 by the silica [36–38]. However, very interesting, the rate constants of dip-coated samples are significantly higher than those of inline functionalized samples for both PA 6 and silica. Via TGA and ICP-OES it was quantified that the 0.12 M DC samples had the same TiO_2 loading as the inline functionalized samples with 5 wt% (for PA 6) and 2 wt% (for silica) (Table 1). The presence of TiO_2 only at the surface of the nanofibers resulted thus, as expected, in a higher degradation rate. Comparing the MB decoloring results to literature, although not always straightforward due to various testing conditions used, it can be stated that both inline

and post-functionalized PA 6 membranes are in line with the results of Daels *et al* [23] and even better than results obtained by Pant *et al* [39] and Kasanen *et al* [40].

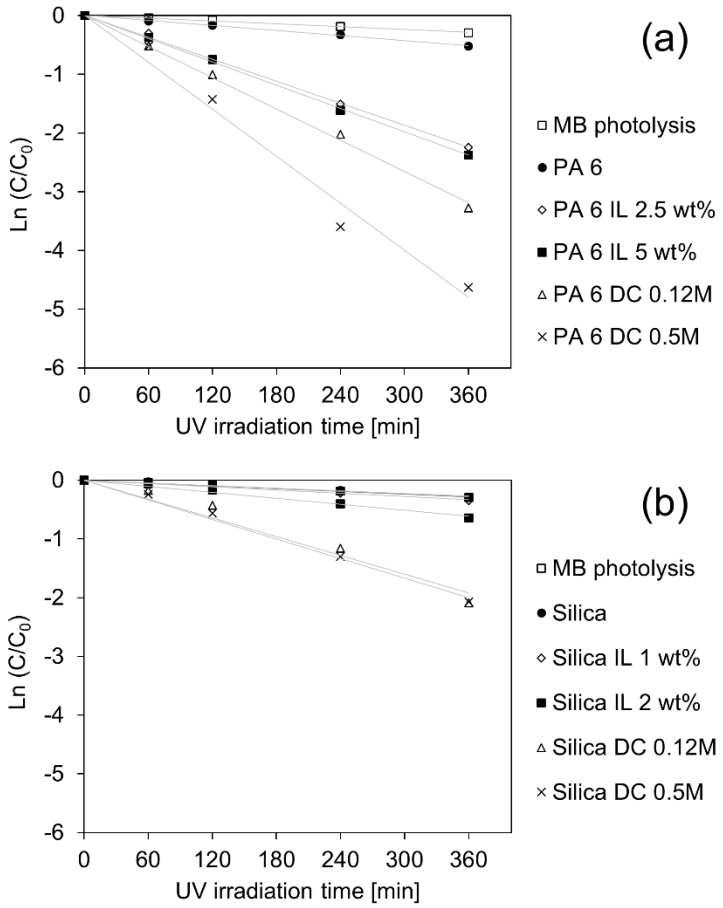

Figure 4 Photolysis of methylene blue solution under UV and removal of aqueous methylene blue solution as a function of time by non-functionalized and TiO_2 functionalized (IL: inline, DC: dip-coating) PA 6 (a) and silica (b) nanofibrous membranes; the amount of TiO_2 added is expressed as wt% for IL samples, for the DC samples the concentration of TiO_2 in the coating solution is denoted in M (mol L^{-1}).

Table 2 Degradation rate constants of aqueous MB solutions in contact with TiO_2 functionalized PA 6 and silica nanofibrous membranes determined via UV-Vis spectroscopy (IL: inline, DC:dip-coating; the amount of TiO_2 added is expressed as wt% for IL samples, for the DC samples the concentration of TiO_2 in the coating solution is denoted in M (mol L^{-1}).

	k [min^{-1}]	R^2	t_{90} [h]		k [min^{-1}]	R^2	t_{90} [h]
MB photolysis	0.0008	0.99	48.2	**MB photolysis**	0.0008	0.99	48.2
PA 6	0.0014	0.99	38.4	**Silica**	0.0008	0.99	48.2
PA 6 IL 2.5 wt%	0.0062	0.99	6.5	**Silica IL 1 wt%**	0.0009	0.99	38.9
PA 6 IL 5 wt%	0.0068	0.99	5.5	**Silica IL 2 wt%**	0.0017	0.99	19.5
PA 6 DC 0.12M	0.0089	0.99	4.3	**Silica DC 0.12M**	0.0053	0.96	6.8
PA 6 DC 0.5M	0.0133	0.98	2.9	**Silica DC 0.5M**	0.0056	0.99	6.6

When evaluating both the photocatalytic results and the morphology/pore blocking of the membranes after functionalization it can be stated that inline functionalization is preferred for PA 6, since pore blocking is a major concern for PA 6 dip-coated membranes. Moreover, inline functionalization results in sufficiently high removal rates. In contrast to PA 6, dip-coating of the silica samples resulted in membranes where no pore blocking was noticed and high removal rates are seen, making post-functionalization thus preferred for silica nanofibrous membranes. Inline functionalization of silica is no valuable option for the decoloring of MB, due to the shielding effect of the silica. This now allows to test the potential of the best membranes for their removal of the contaminant isoproturon which is a current challenge during water treatment.

3.3 Degradation of isoproturon

Isoproturon degradation by both PA 6 and silica nanofibrous samples, functionalized with TiO_2 nanoparticles, was followed via both UV-Vis spectroscopy and LC-MS. Sharma *et al* found that the degradation of isoproturon also followed pseudo first-order kinetics [41,42]. Therefore, the photocatalytic activity was again calculated from the logarithmic plots of the pseudo first-order degradation rate of the isoproturon solutions in contact with the functionalized membranes. The logarithmic plots based on both UV-Vis spectroscopy (Figure 5) and LC-MS (Figure 6) are given and compared.

A clear increase in isoproturon removal was seen upon functionalization with TiO_2 for both PA 6 and silica nanofibrous membranes (Table 3). The same trends were seen as for the MB decoloring. The functionalization of both PA 6 and silica samples with a substantial increased TiO_2 loading was further optimized using inline functionalization for PA 6 (inline 35 wt%) and via dip-coating for silica nanofibrous membranes (hydrophilic silica, 0.34 M TiO_2, 10 min immersion time) to obtain even better degradation rates. Comparing the different PA 6 samples it is seen that inline functionalization with 2.5 wt% resulted in an increased removal compared to non-functionalized samples, furthermore dip-coating with 0.12 M solution even further increased the removal. The highest removal rate was obtained using the 35 wt% inline functionalized PA 6 samples, being the PA 6 sample with the highest TiO_2 load. Silica samples inline functionalized with TiO_2 did not result in a higher removal rate compared to non-functionalized samples, similar to MB decoloring. Again confirming that inline functionalization of silica nanofibrous membranes with TiO_2 is not the preferred method for organic components removal. Functionalization of these silica membranes using dip-coating resulted in much higher degradation rates, resulting in the fastest removal of isoproturon for the hydrophilic dip-coated sample, which is the sample with the highest TiO_2 load. This sample gave the best overall rate constant of all tested samples and therefore it was studied more in-depth using LC-MS (Figure 6 a). Complete removal of isoproturon is seen after 24 hours using a straightforward test set-up. Moreover, to the best of our knowledge this is the first study reporting on TiO_2 functionalized nanofibrous membranes for isoproturon removal.

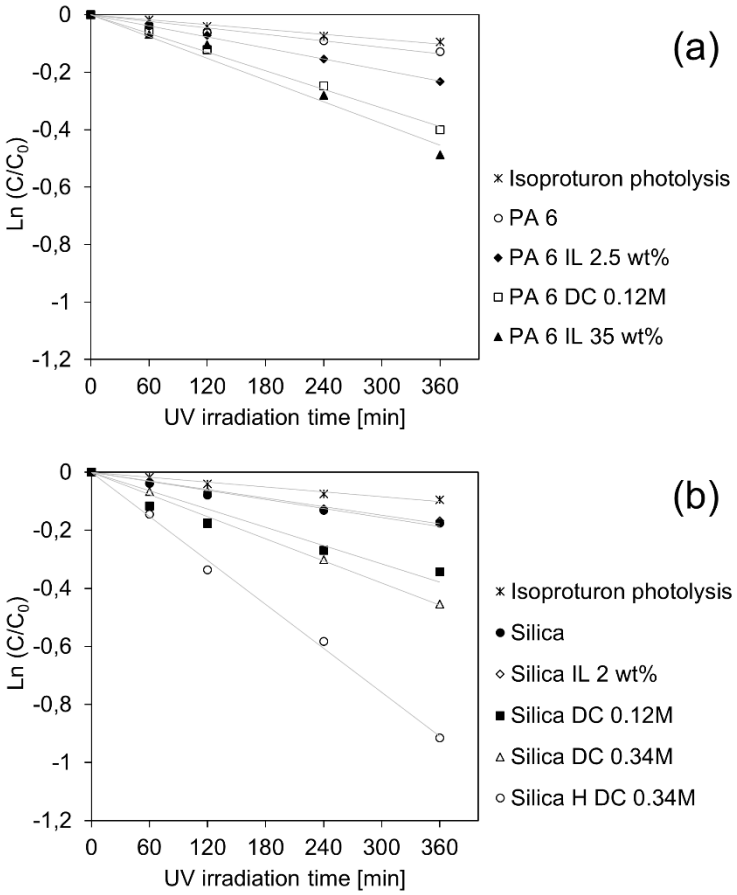

Figure 5 Photolysis of isoproturon solution under UV and removal of aqueous isoproturon solution as a function of time by non-functionalized and TiO_2 functionalized (IL: inline, DC: dip-coating and H: hydrophilic) PA 6 (a) and silica (b) nanofibrous membranes based on UV-Vis spectroscopy; the amount of TiO_2 added is expressed as wt% for IL samples, for the DC samples the concentration of TiO_2 in the coating solution is denoted in M (mol L^{-1}).

Table 3 Degradation rate constants of aqueous isoproturon solutions in contact with TiO_2 functionalized PA6 and silica nanofibrous membranes determined via UV-Vis spectroscopy and LC-MS. (IL: inline, DC: dip-coated and H: hydrophilic); the amount of TiO_2 added is expressed as wt% for IL samples, for the DC samples the concentration of TiO_2 in the coating solution is denoted in M (mol L^{-1}).

	k [min^{-1}]	**R^2**	**t_{90} [h]**		**k [min^{-1}]**	**R^2**	**t_{90} [h]**
UV-Vis							
Isoproturon photolysis	0.0003	0.98	127.8	**Isoproturon photolysis**	0.0003	0.98	127.7
PA 6	0.0004	0.94	127.8	**Silica**	0.0005	0.97	76.4
PA 6 IL 2.5 wt%	0.0006	0.99	64	**Silica IL 2 wt%**	0.0005	0.98	76.5
PA 6 DC 0.12M	0.0011	0.99	38.5	**Silica DC 0.12M**	0.0011	0.91	41.9
PA 6 IL 35 wt%	0.0013	0.97	38.4	**Silica DC 0.34M**	0.0013	0.99	38.3
				Silica H DC 0.34M	0.0025	0.99	12.8
LC-MS							
PA 6 DC 0.12M	0.0015	0.97	19.5	**Silica DC 0.12M**	0.0012	0.97	37.8
PA 6 IL 35 wt%	0.0016	0.99	19.2	**Silica H DC 0.34M**	0.0028	0.99	13.1

Comparing the rate constants obtained via UV-Vis spectroscopy and LC-MS similar results are obtained, with LC-MS resulting in an even slightly higher degradation rate. Indeed a small underestimation of the degradation rate using UV-Vis spectroscopy can be explained by the presence of degradation products absorbing in the same UV region of the electromagnetic spectrum as isoproturon. However, UV-Vis spectroscopy can clearly be a viable fast, easy accessible method to demonstrate the removal of isoproturon in time.

Thus, optimization of inline functionalized PA 6 samples and dip-coated silica samples results in a significant and even complete removal of isoproturon in time. In this research, a basic set-up was used to characterize the isoproturon degradation, to demonstrate the large

potential of these Degussa P25 TiO_2 functionalized nanofibrous membranes for advanced water treatment. These membranes might be used for various organic (micro)pollutants and they are applicable in both membrane separation reactors and contact reactors. PA 6 is the most economical option in non-harsh conditions. However, a slightly slower removal of isoproturon was noted for PA 6 nanofibrous membranes functionalized with TiO_2 (inline 35 wt%) compared to silica (hydrophilic, DC 0.34 M). The best removal rates were obtained with hydrophilic silica nanofibrous membranes functionalized via dipcoating. In addition to the high potential for the degradation of micro-polluants, the ceramic silica nanofibrous membranes offer a high chemical and thermal resistance making them also promising materials for other effluent treatments such as highly acidic effluents.

No other reports on nanofibrous supports for isoproturon removal were found, nevertheless limited research has been carried out on immobilized titanium dioxide on inert non-porous substrates. Verma *et al* immobilized Degussa P25 nanoparticles on an inert glass sheet support, resulting in only 70% removal of isoproturon after 420 hours of exposure to sunlight [43]. The best result on a non-porous support was reported by Losito *et al* [44]. Titanium dioxide-poly(vinylidenefluoride) (TiO_2-PVDF) was deposited on glass substrates by casting or spin-coating, giving 70% up to 90% removal in 5 hours, being in the same order as the 60% removal in 6 hours of our best sample. Our results thus confirm the potential of TiO_2 to remove micro pollutants such as isoproturon. Moreover, a correct immobilization on a nanofibrous matrix results in a functionalized highly porous material, ideal for future reactor set-up design.

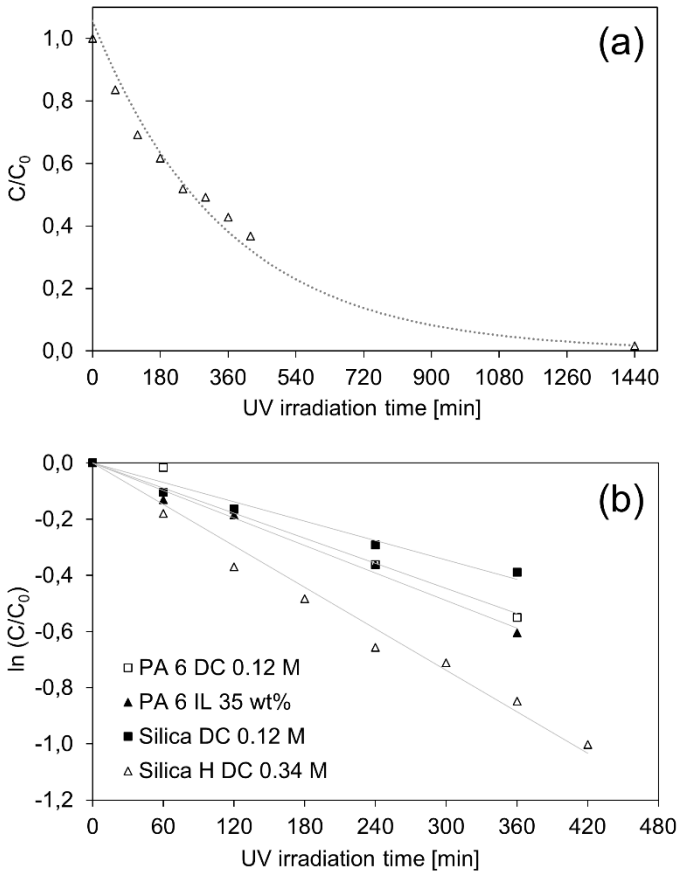

Figure 6 Removal of aqueous isoproturon solution as a function of time by hydrophilic silica nanofibrous membrane dip-coated with 0.34 M TiO_2 solution (a), removal of aqueous isoproturon solution as a function of time by non-functionalized and TiO_2 functionalized PA 6 and silica nanofibrous membranes based on LC-MS measurements (b). (IL: inline, DC: dip-coating and H: hydrophilic); the amount of TiO_2 added is expressed as wt% for IL samples, for the DC samples the concentration of TiO_2 in the coating solution is denoted in M (mol L^{-1}).

4. CONCLUSIONS

Functionalization of polyamide 6 and silica nanofibrous membranes with TiO_2 nanoparticles was optimized via both inline functionalization and dip-coating. Inline functionalization with increased amounts of TiO_2 showed to be the best functionalization method for PA 6, since dip-coating results in pore blocking. For silica, on the contrary, dip-coating was the preferred functionalization method, avoiding shielding of the TiO_2 by the silica shell. Immobilization of

these nanoparticles on these porous supports resulted in highly photocatalytically active membranes, which was verified via their Tauc plots and demonstrated via methylene blue decoloring. Finally, complete removal of isoproturon, a real concern in current water treatment progresses, was established using a basic set-up. By functionalizing a highly porous and flexible support with commercial available TiO_2 nanoparticles, advanced materials were produced showing a high potential to be used for removal of organic (micro)pollutants. Moreover, these membranes can be applied in both membrane separation reactors as contact reactors. PA 6 is assumed to be the most economical and efficient option for non-harsh environments. Silica nanofibrous membranes, on the other hand, can be highly valuable for removal of organic species in industrial, highly acidic effluents.

Supporting Information. Additional information on ICP-OES analysis, XRD analysis and Tauc plot construction. Emission spectrum of Osram Ultra-Vitalux lamp.

Acknowledgements*:* The Agency for Innovation by Science and Technology (IWT) is gratefully acknowledged by J.G. for funding the research through a PhD grant (121241). Nele Daels is acknowledged for her practical guidance.

Funding: This work was supported by the Agency for Innovation by Science and Technology (IWT) [PhD grant number 121241].

REFERENCES

[1] X. Chen, S.S. Mao, Titanium dioxide nanomaterials: Synthesis, properties, modifications and applications, Chem. Rev. 107 (2007) 2891–2959. doi:10.1021/cr0500535.

[2] A. Fujishima, T.N. Rao, D. a. Tryk, Titanium dioxide photocatalysis, J. Photochem.

Photobiol. C Photochem. Rev. 1 (2000) 1–21. doi:10.1016/S1389-5567(00)00002-2.

[3] N. Daels, M. Radoicic, M. Radetic, K. De Clerck, S.W.H. Van Hulle, Electrospun nanofibre membranes functionalised with TiO2 nanoparticles: Evaluation of humic acid and bacterial removal from polluted water, Sep. Purif. Technol. 149 (2015) 488–494. doi:10.1016/j.seppur.2015.06.016.

[4] J.M. Herrmann, Heterogeneous photocatalysis: State of the art and present applications, Top. Catal. 34 (2005) 49–65. doi:10.1007/s11244-005-3788-2.

[5] J. Watté, P. Lommens, G. Pollefeyt, M. Meire, K. De Buysser, I. Van Driessche, Highly Crystalline Nanoparticle Suspensions for Low-Temperature Processing of TiO_2 Thin Films, ACS Appl. Mater. Interfaces. (2016) acsami.6b01684. doi:10.1021/acsami.6b01684.

[6] J. Mo, Y. Zhang, Q. Xu, J.J. Lamson, R. Zhao, Photocatalytic purification of volatile organic compounds in indoor air: A literature review, Atmos. Environ. 43 (2009) 2229–2246. doi:10.1016/j.atmosenv.2009.01.034.

[7] Z. Zhang, C.-C. Wang, R. Zakaria, J.Y. Ying, Role of Particle Size in Nanocrystalline TiO2-Based Photocatalysts, J. Phys. Chem. B. 102 (1998) 10871–10878. doi:10.1021/jp982948+.

[8] G.K. Prasad, G.S. Agarwal, B. Singh, G.P. Rai, R. Vijayaraghavan, Photocatalytic inactivation of Bacillus anthracis by titania nanomaterials, J. Hazard. Mater. 165 (2009) 506–510. doi:10.1016/j.jhazmat.2008.10.009.

[9] R. Loos, G. Locoro, S. Comero, S. Contini, D. Schwesig, F. Werres, P. Balsaa, O. Gans, S. Weiss, L. Blaha, M. Bolchi, B.M. Gawlik, Pan-European survey on the occurrence of

selected polar organic persistent pollutants in ground water, Water Res. 44 (2010) 4115–4126. doi:10.1016/j.watres.2010.05.032.

[10] L. Nitschke, W. Schüssler, Surface water pollution by herbicides from effluents of waste water treatment plants., Chemosphere. 36 (1998) 35–41.

[11] A.R. Ribeiro, O.C. Nunes, M.F.R. Pereira, A.M.T. Silva, An overview on the advanced oxidation processes applied for the treatment of water pollutants defined in the recently launched Directive 2013/39/EU, Environ. Int. 75 (2015) 33–51. doi:10.1016/j.envint.2014.10.027.

[12] M.R. Espino-Estévez, C. Fernández-Rodríguez, O.M. González-Díaz, J. Araña, J.P. Espinós, J.A. Ortega-Méndez, J.M. Doña-Rodríguez, Effect of TiO2-Pd and TiO2-Ag on the photocatalytic oxidation of diclofenac, isoproturon and phenol, Chem. Eng. J. 298 (2016) 82–95. doi:10.1016/j.cej.2016.04.016.

[13] S. Parra, S. Malato, C. Pulgarin, New integrated photocatalytic-biological flow system using supported TiO2 and fixed bacteria for the mineralization of isoproturon, Appl. Catal. B Environ. 36 (2002) 131–144. doi:10.1016/S0926-3373(01)00293-4.

[14] M.N. Chong, B. Jin, C.W.K. Chow, C. Saint, Recent developments in photocatalytic water treatment technology: A review, Water Res. 44 (2010) 2997–3027. doi:10.1016/j.watres.2010.02.039.

[15] M.N. Chong, V. Vimonses, S. Lei, B. Jin, C. Chow, C. Saint, Synthesis and characterisation of novel titania impregnated kaolinite nano-photocatalyst, Microporous Mesoporous Mater. 117 (2009) 233–242. doi:10.1016/j.micromeso.2008.06.039.

[16] Z. Sun, Y. Chen, Q. Ke, Y. Yang, J. Yuan, Photocatalytic degradation of cationic azo

dye by TiO2/bentonite nanocomposite, J. Photochem. Photobiol. A Chem. 149 (2002) 169–174. doi:10.1016/S1010-6030(01)00649-9.

[17] M.R. Espino-Estévez, C. Fernández-Rodríguez, O.M. González-Díaz, J.A. Navío, D. Fernández-Hevia, J.M. Doña-Rodríguez, Enhancement of stability and photoactivity of TiO<inf>2</inf> coatings on annular glass reactors to remove emerging pollutants from waters, Chem. Eng. J. 279 (2015) 488–497. doi:10.1016/j.cej.2015.05.038.

[18] R.S. Barhate, S. Ramakrishna, Nanofibrous filtering media: Filtration problems and solutions from tiny materials, J. Memb. Sci. 296 (2007) 1–8. doi:10.1016/j.memsci.2007.03.038.

[19] S. Ramakrishna, K. Fujihara, W.E. Teo, T. Yong, Z. Ma, R. Ramaseshan, Electrospun nanofibers: Solving global issues, Mater. Today. 9 (2006) 40–50. doi:10.1016/S1369-7021(06)71389-X.

[20] A. Greiner, J.H. Wendorff, Electrospinning: A fascinating method for the preparation of ultrathin fibers, Angew. Chemie - Int. Ed. 46 (2007) 5670–5703. doi:10.1002/anie.200604646.

[21] D. Li, Y. Xia, Electrospinning of nanofibers: Reinventing the wheel?, Adv. Mater. 16 (2004) 1151–1170. doi:10.1002/adma.200400719.

[22] N. Daels, S. De Vrieze, I. Sampers, B. Decostere, P. Westbroek, a. Dumoulin, P. Dejans, K. De Clerck, S.W.H. Van Hulle, Potential of a functionalised nanofibre microfiltration membrane as an antibacterial water filter, Desalination. 275 (2011) 285–290. doi:10.1016/j.desal.2011.03.012.

[23] N. Daels, M. Radoicic, M. Radetic, S.W.H. Van Hulle, K. De Clerck, Functionalisation

of electrospun polymer nanofibre membranes with TiO2 nanoparticles in view of dissolved organic matter photodegradation, Sep. Purif. Technol. 133 (2014) 282–290. doi:10.1016/j.seppur.2014.06.040.

[24] J. Kim, B. Van Der Bruggen, The use of nanoparticles in polymeric and ceramic membrane structures: Review of manufacturing procedures and performance improvement for water treatment, Environ. Pollut. 158 (2010) 2335–2349. doi:10.1016/j.envpol.2010.03.024.

[25] Z. Ma, H. Ji, Y. Teng, G. Dong, J. Zhou, D. Tan, J. Qiu, Engineering and optimization of nano- and mesoporous silica fibers using sol-gel and electrospinning techniques for sorption of heavy metal ions, J. Colloid Interface Sci. 358 (2011) 547–553. doi:10.1016/j.jcis.2011.02.066.

[26] S. Wu, F. Li, Y. Wu, R. Xu, G. Li, Preparation of novel poly(vinyl alcohol)/SiO(2) composite nanofiber membranes with mesostructure and their application for removal of Cu(2+) from waste water., Chem. Commun. (Camb). 46 (2010) 1694–1696. doi:10.1039/b925296g.

[27] R. Xu, M. Jia, Y. Zhang, F. Li, Sorption of malachite green on vinyl-modified mesoporous poly(acrylic acid)/SiO2 composite nanofiber membranes, Microporous Mesoporous Mater. 149 (2012) 111–118. doi:10.1016/j.micromeso.2011.08.024.

[28] S. Ramakrishna, R. Jose, P.S. Archana, A.S. Nair, R. Balamurugan, J. Venugopal, W.E. Teo, Science and engineering of electrospun nanofibers for advances in clean energy, water filtration, and regenerative medicine, J. Mater. Sci. 45 (2010) 6283–6312. doi:10.1007/s10853-010-4509-1.

[29] J. Geltmeyer, J. De Roo, F. Van den Broeck, J.C. Martins, K. De Buysser, K. De Clerck,

The influence of tetraethoxysilane sol preparation on the electrospinning of silica nanofibers, J. Sol-Gel Sci. Technol. 77 (2016) 453–462. doi:10.1007/s10971-015-3875-1.

[30] J. Geltmeyer, L. Van der Schueren, F. Goethals, K. De Buysser, K. De Clerck, Optimum sol viscosity for stable electrospinning of silica nanofibres, J. Sol-Gel Sci. Technol. 67 (2013) 188–195. doi:10.1007/s10971-013-3066-x.

[31] J. Geltmeyer, G. Vancoillie, I. Steyaert, B. Breyne, G. Cousins, K. Lava, R. Hoogenboom, K. De Buysser, K. De Clerck, Dye Modification of Nanofibrous Silicon Oxide Membranes for Colorimetric HCl and NH3 Sensing, Adv. Funtional Mater. (2016) 1–10. doi:10.1002/adfm.201602351.

[32] S. de Vrieze, B. De Schoenmaker, K. De Clerck, Morphologic study of steady state electrospun polyamide 6 nanofibres, J. Appl. Polym. Sci. 119 (2011) 2984–2990. doi:10.1002/app.

[33] C. Mit-uppatham, M. Nithitanakul, P. Supaphol, Ultrafine electrospun polyamide-6 fibers: Effect of solution conditions on morphology and average fiber diameter, Macromol. Chem. Phys. 205 (2004) 2327–2338. doi:10.1002/macp.200400225.

[34] J. Zeng, H. Haoqing, A. Schaper, J.H. Wendorff, A. Greiner, Poly-L-lactide nanofibers by electrospinning – Influence of solution viscosity and electrical conductivity on fiber diameter and fiber morphology, E-Polymers. 3 (2003) 1–9. doi:10.1515/epoly.2003.3.1.102.

[35] R. López, R. Gómez, Band-gap energy estimation from diffuse reflectance measurements on sol-gel and commercial TiO2: A comparative study, J. Sol-Gel Sci. Technol. 61 (2012) 1–7. doi:10.1007/s10971-011-2582-9.

[36] A.M. El-Toni, S. Yin, T. Sato, Control of silica shell thickness and microporosity of titania-silica core-shell type nanoparticles to depress the photocatalytic activity of titania, J. Colloid Interface Sci. 300 (2006) 123–130. doi:10.1016/j.jcis.2006.03.073.

[37] I.A. Siddiquey, T. Furusawa, M. Sato, K. Honda, N. Suzuki, Control of the photocatalytic activity of TiO2 nanoparticles by silica coating with polydiethoxysiloxane, Dye. Pigment. 76 (2008) 754–759. doi:10.1016/j.dyepig.2007.01.020.

[38] A.M. El-Toni, S. Yin, T. Sato, T. Ghannam, M. Al-Hoshan, M. Al-Salhi, Investigation of photocatalytic activity and UV-shielding properties for silica coated titania nanoparticles by solvothermal coating, J. Alloys Compd. 508 (2010) L1–L4. doi:10.1016/j.jallcom.2013.01.001.

[39] H.R. Pant, B. Pant, P. Pokharel, H.J. Kim, L.D. Tijing, C.H. Park, D.S. Lee, H.Y. Kim, C.S. Kim, Photocatalytic TiO2-RGO/nylon-6 spider-wave-like nano-nets via electrospinning and hydrothermal treatment, J. Memb. Sci. 429 (2013) 225–234. doi:10.1016/j.memsci.2012.11.025.

[40] J. Kasanen, J. Salstela, M. Suvanto, T.T. Pakkanen, Photocatalytic degradation of methylene blue in water solution by multilayer TiO2 coating on HDPE, Appl. Surf. Sci. 258 (2011) 1738–1743. doi:10.1016/j.apsusc.2011.10.028.

[41] M.V.P. Sharma, V. Durgakumari, M. Subrahmanyam, Solar photocatalytic degradation of isoproturon over TiO2/H-MOR composite systems, J. Hazard. Mater. 160 (2008) 568–575. doi:10.1016/j.jhazmat.2008.03.042.

[42] M. V. Phanikrishna Sharma, V. Durga Kumari, M. Subrahmanyam, Photocatalytic degradation of isoproturon herbicide over TiO2/Al-MCM-41 composite systems using

solar light, Chemosphere. 72 (2008) 644–651. doi:10.1016/j.chemosphere.2008.02.042.

[43] A. Verma, N.T. Prakash, A.P. Toor, Photocatalytic degradation of herbicide isoproturon in TiO2 aqueous suspensions: study of reaction intermediates and degradation pathways, Environ. Prog. Sustain. Energy. 33 (2014) 402–409. doi:10.1002/ep.

[44] I. Losito, A. Amorisco, F. Palmisano, P.G. Zambonin, X-ray photoelectron spectroscopy characterization of composite TiO 2-poly(vinylidenefluoride) films synthesised for applications in pesticide photocatalytic degradation, Appl. Surf. Sci. 240 (2005) 180–188. doi:10.1016/j.apsusc.2004.06.068.

Supporting Information

TiO_2 functionalized nanofibrous membranes for removal of organic (micro)pollutants

Jozefien Geltmeyer[a], Helena Teixido[a], Mieke Meire[b], Thibaut Van Acker[d], Koen Deventer[c],

*Franck Vanhaecke[d], Stijn Van Hulle[e], Klaartje De Buysser[b], Karen De Clerck[a,]**

[a] Fibre and Colouration Technology Research Group, Department of Textiles, Faculty of Engineering and Architecture, Ghent University, Technologiepark 907, 9052 Ghent, Belgium, Karen.DeClerck@UGent.be

[b] Sol-gel Centre for Research on Inorganic Powders and Thin Films Synthesis, Department of Inorganic and Physical Chemistry, Faculty of Sciences, Ghent University, Krijgslaan 281 S3, 9000 Ghent, Belgium

[c] Doping Control Laboratory, Ghent University, Technologiepark 30, 9052 Ghent, Belgium

[d] Department of Analytical Chemistry, Faculty of Sciences, Ghent University, Krijgslaan 281 S12, 9000 Ghent, Belgium

[e] LIWET, Department of Industrial Biological Sciences, Ghent University Campus Kortrijk, Graaf Karel de Goedelaan 5, B-8500 Kortrijk, Belgium

ICP-OES analysis. Inductively Coupled Plasma Optical Emission Spectroscopy (ICP-OES) was carried out to quantify the amount of titanium present in or on the membranes. To ± 10 mg of TiO_2 functionalized PA 6 nanofibrous samples, 4 mL of concentrated HNO_3 and 1 mL of concentrated H_2SO_4 was added, followed by an acid digestion in a Milestone MLS-1200 microwave oven. After digestion, 100 µL of the internal standard (IS) was added to 500 µL of the obtained solution, and further diluted to a volume of 10 mL with milli-Q water. To ± 20 mg of TiO_2 functionalized silica nanofibers 2 mL of concentrated HNO_3 and 1 mL of concentrated HF was added. This was followed by an acid digestion in closed Savillex beakers (24 hours at 90 °C). Next, the samples were evaporated and again dissolved in 2 mL of 10 % HNO_3, followed by an appropriate dilution for each sample (Silica 0.2 wt%: 1 mL of sample + 100 µL IS – dilution to 10 mL with 1 % HNO_3, silica 2 wt % and silica DC 0.12M: 500 µL of sample + 100 µL IS – dilution to 10 mL with 1 % HNO_3). Analysis of all samples was carried out with an ICP-OES (Spectra Arcos).

XRD analysis. Previous to the X-Ray Diffraction (XRD) analysis, the sample were heated to 1000 °C for 4 hours. The samples were milled and side-loaded into the sample holder. The XRD data were collected on a Thermo Scientific ARL X'tra Diffractometer equipped with a Peltier cooled detector. Samples were measured in θ-2θ geometry over an angular range of 5-70 °2θ (CuKα radiation) using a 0.02 °2θ step size and 1 s/step counting time. The Rietveld method for whole-powder pattern fitting was used to investigate the ratios of the crystalline phases (SiO_2 vs $TiSiO_4$). Topas Academic V4.1 software was used for Rietveld refinement [Coelho, A.A., Topas Academic version 4.1. 2007.]. The refined parameters were the measurement specific or sample displacement error, a cosine Chebyshev function of 12 polynomial terms for background correction, phase specific scale factors, unit cell parameters and Lorentzian peak shape broadening parameters.

Tauc plot construction. Diffuse reflectance spectra of the functionalized samples with an integrating sphere were collected with a Lambda 900 UV-Vis spectrophotometer (Perkin-Elmer). The non-functionalized samples were used for the background spectra. Out of these spectra a Tauc plot was made using the method described by López *et al* [35]. The optical absorption data near the band edge can be used to determine the optical band gap of a crystalline semiconductor:

$$\alpha h\nu = A\,(h\nu - E_g)^n \quad (1)$$

With α the absorption constant, ν the light frequency [s^{-1}], E_g the band gap energy [eV], h the Planck constant [J.s] and A is a proportionality constant. n determines the characteristics of the transition in the semi-conductor. For commercial Degussa P25 TiO_2 nanoparticles, the use of equation (1) with n = 2 for indirect allowed transitions is suggested [35]. The absorption constant α is proportional with the Kubelka-Munk function F(R), with R the reflectance:

$$F\,(R) = \frac{(1-R)^2}{2R} \quad (2)$$

The values of the band gap energy can be determined by the construction of the Tauc plot by plotting $(F(R)*h\nu)^{1/n}$ as a function of hν (photon energy). The band gap energy is then determined by extrapolating the straightest line to the hν axis intercept.

Figure S1 Light emission spectrum of Osram Ultra-Vitalux lamp